12-30-2019

# A Technique for Calculating Flexural Rigidity of Nonlinear Systems

Chase Hartquist
*Washington University in St. Louis*

# A Technique for Calculating Flexural Rigidity of Nonlinear Systems

**Chase Hartquist**

**Washington University McKelvey School of Engineering, St. Louis, MO**

**December 2019**

## Introduction

Geometric, kinematic, force, and material nonlinearity arise in manufactured products. Flexural rigidity, or relative stiffness of a beam, cannot be measured accurately for flexible, composite medical devices like catheters and sheaths using linear beam theory because they undergo high deformations when subject to relatively small loads. Surgeons depend on the relative stiffness of their catheters to determine the maneuverability of their devices.

For neurovascular interventions, surgeons rely on stiffness to determine if their catheter can navigate arduous vasculature, especially around the aortic arch[1]. Navigation has become increasingly difficult as surgeons have adopted the transradial approach to neurovascular angioplasty procedures. In these procedures, surgeons must steer their guide catheter through the radial artery, across narrow bends through the subclavian artery, and around the aortic arch. It is unrealistic to consistently use particularly flexible catheters since they do not provide enough support to guide medical devices to the brain. To overcome this issue, surgeons pair flexible intermediate guide catheters with stiffer sheaths in a coaxial system. They navigate the guide catheter into position, run the stiff sheath over the guide catheter, and send more devices (microcatheters, stents, coils, etc.) through that system. Medical device companies now commonly design catheters with sections that vary in stiffness throughout the length of the catheter to help overcome these issues[2]. Although the relative stiffness of these devices are critical to the success of the procedure, stiffness values for these devices are unknown to surgeons.

More generally, cardiovascular, peripheral vascular, and other general vascular surgeons experience similar difficulty in selecting catheters to navigate other arterial systems. Cardiovascular surgeons experience similar difficulty navigating bends through the aortic arch for different procedures. Beyond vascular surgery, flexural rigidity calculations are important throughout mechanical analysis, and these calculations become especially difficult for

manufactured products with soft or composite materials. Previous studies have found flexural rigidity calculations of thin films for aerospace engineering[3], of flat plates in mountains for geophysics[4], of microtubules for cell biophysics[5], and of jute fibers and yarns[6].

Euler-Bernoulli and Timoshenko beam theories provide relatively accurate approximations for beams under small deformations[7]. Applications of these theories are fitting to measure the flexural rigidity of catheters and other nonlinear systems. Beams with flexible materials undergoing large deformations require more complicated definitions to solve for flexural rigidity through deflection analysis. A nonlinear approach to beam theory does provide a more accurately measured flexural rigidity for high deformations than linear beam theory[8]. By applying the definition of curvature to the general equation for Euler-Bernoulli beam theory, the flexural rigidity can be calculated accurately.

Other techniques have been applied to manufactured systems to measure mechanical properties of catheters and other medical devices[9]. Previous studies found the flexural rigidity of central venous catheters based on deflections[10,11], which differs from the angle calculations used in this research. Another method from previous studies examines the buckling load of the device when the force is applied axially[12,13]. Yet another group compared stiffness between catheters based on the critical angle at which the catheter could physically bend[14]. These methods for measuring flexural rigidity are distinctly different from the technique used in this research, which instead measures the value based on the angle of rotation where the point load is applied.

For measurement of manufactured products, the flexural rigidity can be calculated through image analysis paired with the nonlinear application of the general beam theory equation. Flexural rigidity can be found by examining the mechanical reaction of a fixed-free beam under a given load. This technique was tested using finite element analysis in COMSOL by measuring angles via displacements using the software applications and through image analysis of the deflection provided by the software. These values were compared to calculated flexural rigidity values, which are based on the elastic modulus and second area moment of inertia of the cross section. This strategy provides researchers with an accurate means to measure the flexural rigidity of medical devices like catheters that undergo large deformations under applied forces.

**Methods**

To determine flexural rigidity in these experiments, linear and nonlinear beam theory equations were used in tandem to find values to compare to the actual value. Equation 1 below shows the general static form for linear and nonlinear beam theory.

$$M = -EI\kappa \tag{1}$$

Where $M$ is the applied moment $[Nm]$, $E$ is the Young's modulus of the material $[N/m^2]$, $I$ is second area moment of inertia of the cross section $[kg\,m^2]$, and $\kappa$ is the definition of curvature $[1/m]$. The combined term $EI$ is defined as flexural rigidity $[Ncm^2]$. Equation 2 below shows an assumption made to determine the static form of Euler-Bernoulli beam theory for linear applications.

$$\kappa = -\frac{d^2w}{dx^2} \tag{2}$$

Where $w(x)$ is the equation describing the deformation of the beam, $\frac{dw}{dx}$ is the slope of the beam, and $\frac{d^2w}{dx^2}$ is the derivative of the slope of the beam. To then solve for the flexural rigidity of the beam, the linear form of curvature is substituted into Eq. 1. The complete derivation for the final form of this equation can be found in Appendix A. Equation 3 shows the final form used to solve for the linear approximation of the flexural rigidity of the beam.

$$EI = \frac{1}{2tan\theta}(FL^2) \tag{3}$$

Where $F$ is the force $[N]$, $L$ is the length from the fixed end to the applied force $[m]$, and $\theta$ is the angle of rotation of the beam at the point of the applied load relative to horizontal [°]. To solve the nonlinear application of beam theory for flexural rigidity, the exact definition of curvature is used in Eq. 1. Equation 4 shows this definition.

$$\kappa = \frac{-\frac{d^2w}{dx^2}}{(1+(\frac{dw}{dx})^2)^{\frac{3}{2}}} \tag{4}$$

The full derivation for the nonlinear form of this equation can be found in Appendix A. Equation 5 shows the final nonlinear derived form for flexural rigidity.

$$EI = \frac{(1+(tan\theta)^2)^{\frac{1}{2}}}{2tan\theta}(FL^2) \tag{5}$$

The final forms of both Eq. 3 and Eq. 5 can be nondimensionalized and described by the term $\frac{FL^2}{2EI}$. The results of this nondimensionalization are shown below in Eq. 6 and Eq. 7 for the linear and nonlinear forms, respectively.

$$\frac{FL^2}{2EI} = tan\theta \tag{6}$$

$$\frac{FL^2}{2EI} = \frac{tan\theta}{(1+(tan\theta)^2)^{\frac{1}{2}}} \tag{7}$$

To show the reliability of the supporting equations, the COMSOL model was used to first test displacements of a 450 mm long tube-shaped structure subjected to a load applied 420 mm from the fixed end of the fixed-free beam. The angle deflection, $\theta$, could then be derived from trigonometry comparing the displacement at the point of the load ($x = 420\ mm$) and the displacement at the end of the beam ($x = 450\ mm$). Note that gravity was not applied in this simulation. The calculated angel could then be applied in Eq. 3 and Eq. 5 to solve for the flexural rigidity of the beam. The ensuant value was then compared to the actual flexural rigidity, which was calculated using the elastic modulus and second area moment of inertia provided by the COMSOL software for the beam constructed. This value was calculated for the beam subject to different loads: $0.025\ N$, $0.05\ N$, $0.1\ N$, $0.125\ N$ and $0.15\ N$. Table 1 below shows the dimensions and material properties of the tube used throughout the model.

**Table 1 Listed are the material properties and dimensions that were tested in the COMSOL model.**

| ID/OD [mm] | I [mm$^4$] | Material | E [GPa] | EI [Ncm$^2$] |
|---|---|---|---|---|
| 1.778/2.1 | 0.4641 | PTFE | 0.4000 | 1.856 |

To verify the validity of these calculations for finite element analysis, a convergence test was run on the data. Results were plotted for the beam designed with 9 different mesh sizes; the number of degrees of freedom varied from 2238 to 423906 degrees of freedom. The force was applied 30 mm from the fixed end of the 35 mm fixed-free beam. These tests were run across the same range of forces listed before along a beam with the same properties as were described in Table 1.

The linear and nonlinear results from the initial COMSOL displacement test were then converted to a dimensionless graph to show the relationship between the dimensionless

quantities derived in Eqs. 6 and 7. This graph is designed to show the relationship between the linear, nonlinear, and actual calculations relating $\frac{FL^2}{2EI}$ and $\theta$.

Next, another dimensionless study was run to show how the nonlinear formulation stands based on the length of the beam ($L$) relative to the diameter ($D$). The resulting nonlinear calculations were performed using the same displacements tests for beams with quantities $\frac{D}{L} = .5$ and $\frac{D}{L} = .005$. These beams had the same parameters as were described in Table 1, but the loads were applied at 4.2 mm and 420 mm from the fixed end on 4.5 mm and 450 mm fixed-free beams, respectively. The results, along with the correct values calculated from the material and geometric properties of the beam, were compared on another dimensionless graph comparing $\frac{FL^2}{2EI}$ and $\theta$.

After testing the reliability of the governing equations and software in this model, an image analysis technique was used to show how effective this derivation applies to calculating flexural rigidity of manufactured products. The image analysis was performed on images taken from the COMSOL modelling software and compared to the calculated value. Once the beam was designed and a fixed boundary condition was applied, a point force was applied to the free end of the beam. Figure 1 below shows a sample beam under deflection from the applied load.

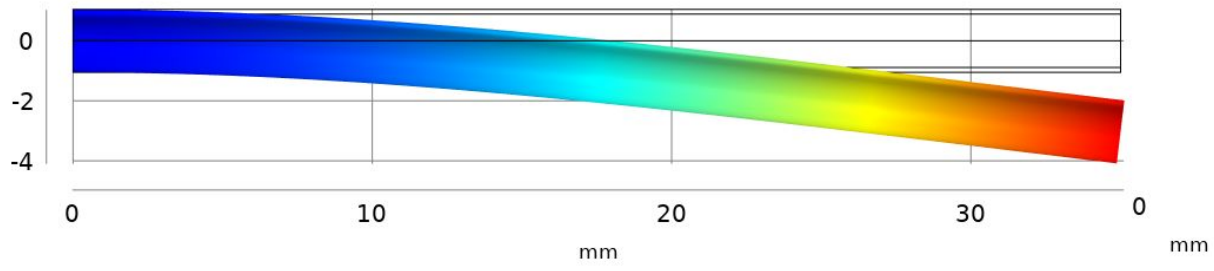


**Fig. 1 Sample image for a 35 mm beam deflection in COMSOL**

This was repeated under $0.025\,N$, $0.05\,N$, $0.1\,N$, and $0.125\,N$ loads applied 30 mm from the fixed end of a 35 mm beam. Images resembling Fig. 1 under each load were then analyzed using ImageJ software to find $\theta$.

**Results**

The initial test in COMSOL was completed by finding the difference in displacements on two points of the beam subject to $0.25\,mN$, $0.5\,mN$, $1\,mN$, $1.25\,mN$ and $1.5\,mN$ forces. Figure 2 below displays the resulting flexural rigidity values based on the angle, $\theta$, of deflection. These measured values are compared to the line that describes the actual flexural rigidity of the beam, which was calculated in Table 1 as $1.856\,Ncm^2$. The beam was tested under finite element analysis using 5744973 degrees of freedom.

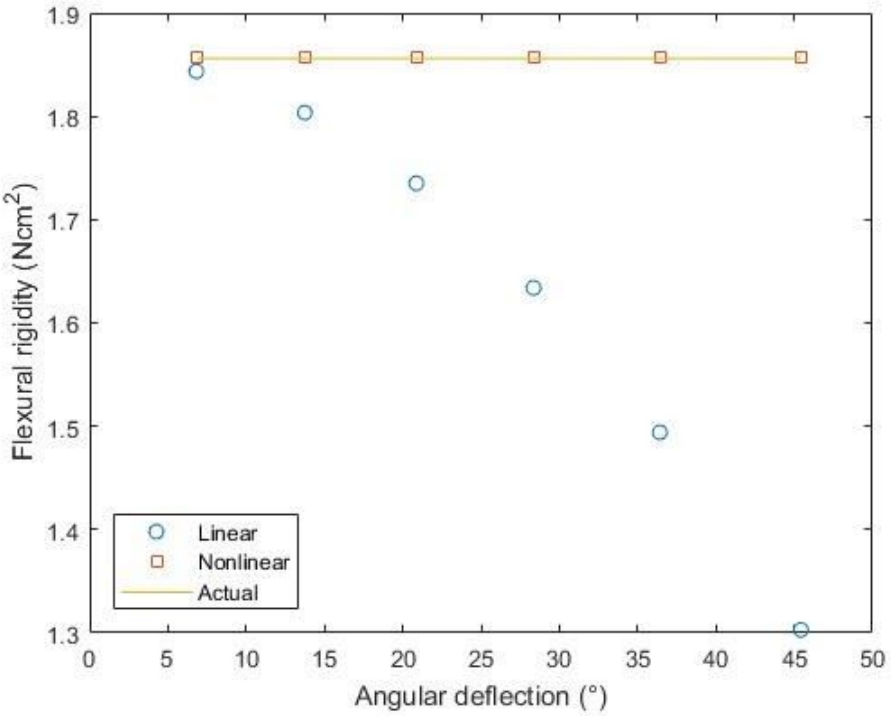


**Fig. 2 Linear and nonlinear flexural rigidity calculations using COMSOL displacements to measure angles based on forces applied 420 mm from the fixed end of a 450 mm fixed-free beam**

Following the initial COMSOL displacement test, a convergence test was conducted for different mesh sizes. Figure 3 shows the resulting flexural rigidity calculations based on the number of degrees of freedom constructed in the design.

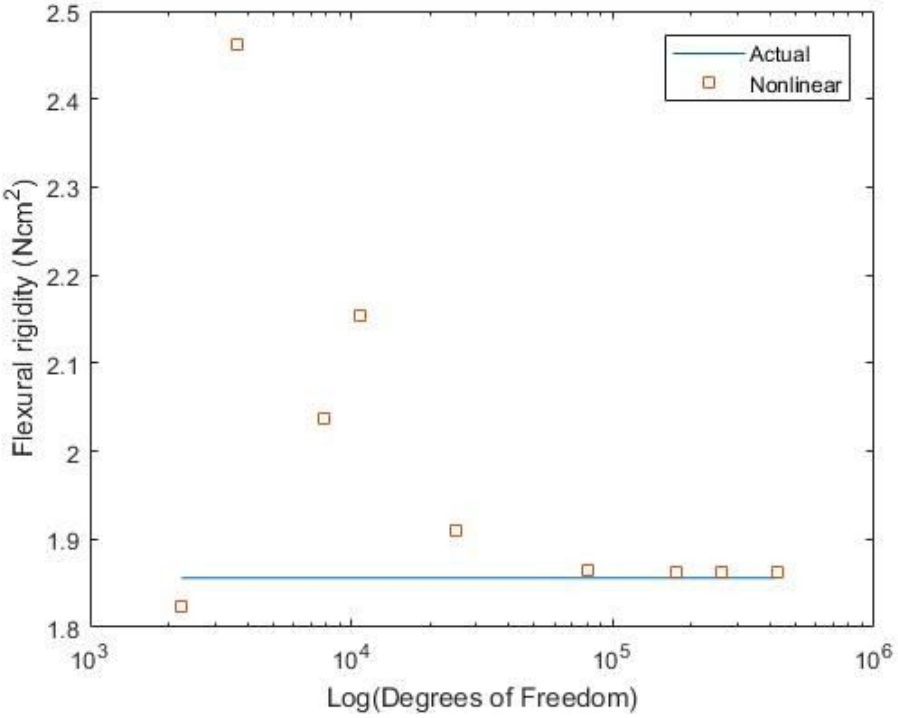


**Fig. 3 Convergence test based on nonlinear calculations from a point force applied 30 mm from the fixed end of a 35 mm fixed-free beam**

A dimensionless graph was then extracted from the data collected in Fig. 1 comparing the linear and nonlinear beam theory calculations to the actual values based on the geometry and material properties of the beam. Figure 4 below shows the results of this comparison, which also relates the nondimensionalized quantities described in Eqs. 6 and 7.

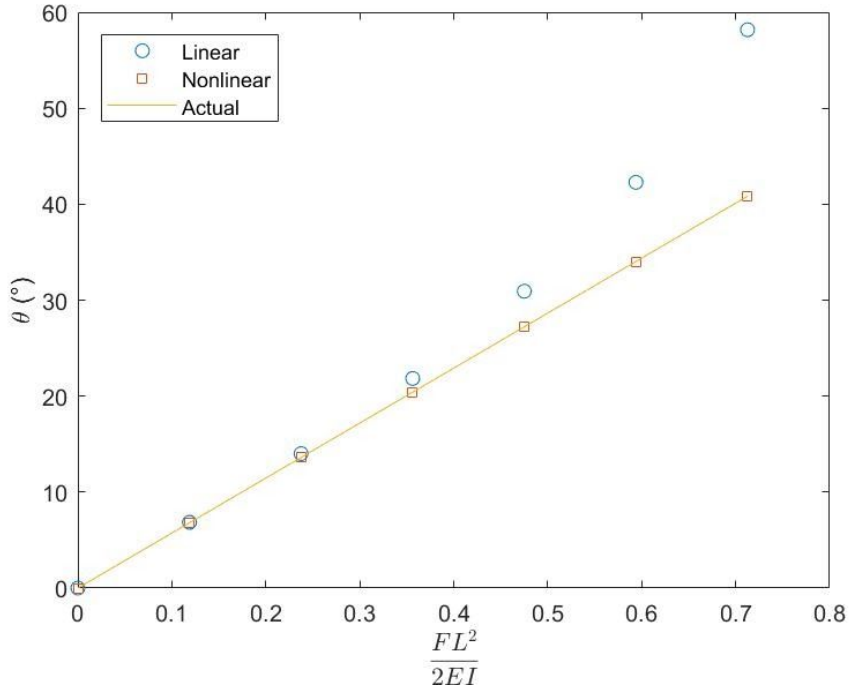


**Fig. 4 Nondimensionalized comparison of linear to nonlinear calculations based where point forces are applied 420 mm from the fixed end of a 420 mm fixed-free beam**

Another dimensionless graph was derived to show how the nonlinear formulations apply to beams based on their diameter to length ratio. Figure 5 below shows this relation, which compares these changing ratios to the actual dimensionless angle calculations of the beam derived from its inherent material and geometric properties.

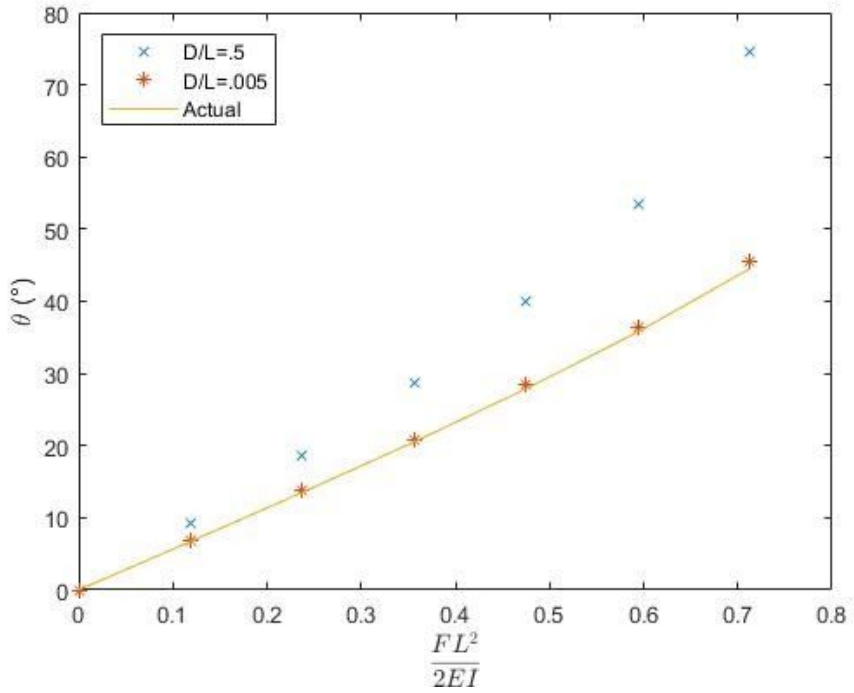


**Fig. 5 Nondimensionalized comparison of nonlinear calculations of beams with diameter (D) to length (L) ratios of .5 and .005**

For the image analysis technique, the tube designed in COMSOL was subjected to loads of $0.025\ N$, $0.05\ N$, $0.1\ N$, and $0.125\ N$. Figure 6 below displays the resulting flexural rigidity values based on the angle, $\theta$, of deflection. These measured values are compared to the line representing the actual flexural rigidity of the beam, which was calculated in Table 1 as $1.856\ Ncm^2$.

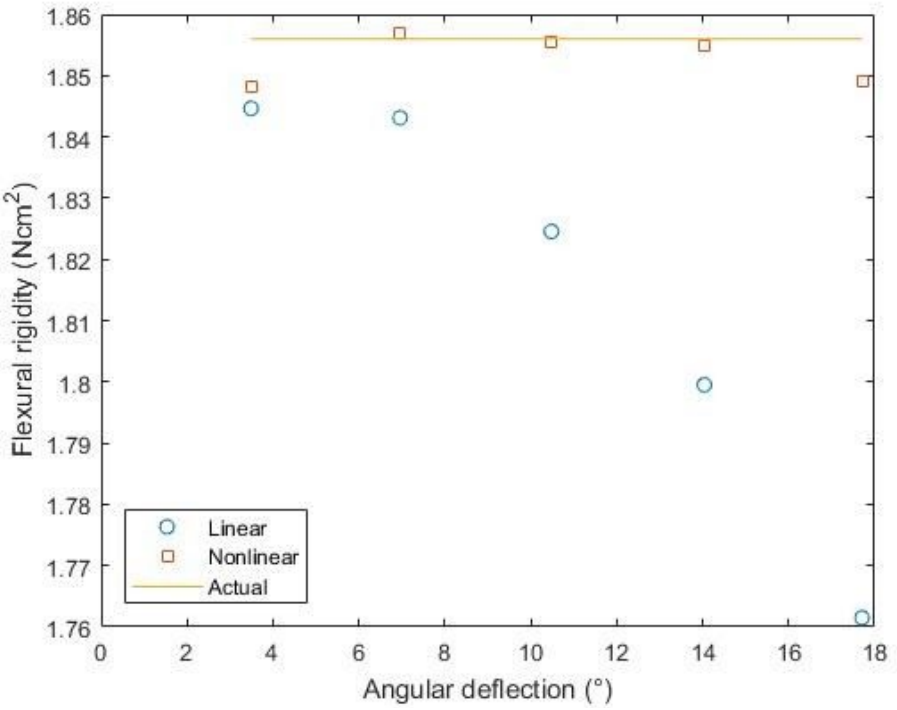


**Fig. 6 Linear and nonlinear flexural rigidity calculations using image analysis to measure the angles from forces applied 30 mm from the fixed end of a 35 mm fixed-free beam**

Table 2 shows the resulting flexural rigidity values measured for each force using both the image analysis and COMSOL displacement test of loads applied 30 mm from the fixed end of a 35 mm fixed-free beam. The linear values were calculated using Eq. 3, and the nonlinear values were calculated using Eq. 5.

**Table 2 Flexural rigidity values are calculated linearly and nonlinearly based on the force applied 30 mm from the free end of the 35 mm fixed-free beam**

| Force [N] | Image Analysis Technique | | COMSOL Displacement Test | | EI [Ncm$^2$] |
|---|---|---|---|---|---|
| | Linear [Ncm$^2$] | Nonlinear [Ncm$^2$] | Linear [Ncm$^2$] | Nonlinear [Ncm$^2$] | |
| .025 | 1.845 | 1.848 | 1.859 | 1.862 | 1.856 |
| .050 | 1.843 | 1.857 | 1.848 | 1.862 | 1.856 |
| .075 | 1.825 | 1.855 | 1.831 | 1.862 | 1.856 |
| .100 | 1.799 | 1.849 | 1.807 | 1.862 | 1.856 |
| .125 | 1.761 | 1.849 | 1.775 | 1.862 | 1.856 |

## Discussion

The calculated flexural rigidity values using linear and nonlinear beam theory reflect the expected trend based on the analysis performed. Since linear beam theory makes approximations for small angles, it does not account for nonlinearity that arises once the beam bends at a high angle. Therefore, when measuring the flexural rigidity using linear beam theory, it is expected that the value would become more inaccurate as the angle increases. This is shown in the COMSOL displacement data, which displays consistently accurate nonlinear terms and shows linear terms that become less accurate with higher angle changes. It is noteworthy that the linear terms did stay within 7 percent of the expected outcome when subjected to an angle change of 20.9°; however, the nonlinear values were consistently within .1 percent error throughout the displacement test.

The convergence test showed that the accuracy of the displacement test improves with an increase in the number of degrees of freedom used in the finite element analysis, which was expected. There were noticeable inconsistencies between the lower degrees of freedom, which can be attributed to the variation in finite element composition as the size of the elements changed. The convergence test showed that the accuracy of the calculations significantly improves as a function of the number of degrees of freedom of the design in COMSOL.

The dimensionless results shown in Fig. 5 show the expected importance of beam length when calculating deflections using beam theory. It is expected that a beam with a large diameter to length ratio would not follow the trends of the theory since this technique does not account for the shear effects that dominate in relatively short beams. These results show that a small diameter to length ratio provides a more accurate measurement.

The results of the initial COMSOL displacement test are also shown in the image analysis data. Under $0.025\,N$, $0.05\,N$ and $.075\,N$ forces, the calculated linear flexural rigidity values were $1.845\,Ncm^2$ and $1.843\,Ncm^2$, $1.825\,Ncm^2$, respectively. These values are within two percent of the actual flexural rigidity, which is $1.856\,Ncm^2$. However, under the larger $0.1\,N$ and $0.125\,N$ forces, the calculated flexural rigidity values were significantly lower. They measured $1.799\,Ncm^2$ and $1.761\,Ncm^2$, respectively. The nonlinear beam theory accounts for the high angle changes. Therefore, when measuring flexural rigidity using nonlinear beam theory, it is expected that the flexural rigidity calculations will remain consistently accurate at high deflection angles. The data does show that this is consistent. When subject to $0.025\,N$, $0.05\,N$, $0.075\,N$, $0.1\,N$ and $0.125\,N$ forces, the calculated nonlinear flexural rigidity values were $1.848\,Ncm^2$, $1.857\,Ncm^2$, $1.855\,Ncm^2$, $1.855\,Ncm^2$, and $1.849\,Ncm^2$, respectively. These values remain consistently under one percent error from the actual flexural rigidity value of $1.856\,Ncm^2$. This shows that the nonlinear beam theory application provides a more accurate flexural rigidity value than linear beam theory. This method is preferable to using linear beam theory for image analysis.

These results are subject to error due to the software capabilities and human measurement error. For the COMSOL modeling software, there are errors associated with modeling a complex system as a series of finite elements. The convergence test performed in the study (shown in Fig. 3) provides insight into how accurately the software approximates with increasing degrees of freedom. Also, the image analysis technique does provide another source of error in pixelation. Exact angles can only be approximated from the image due to limitations of the images and the image analysis technology. This source of error did not significantly change the outcome of the experiments, which showed the the nonlinear calculations were consistent with actual outcomes.

**Acknowledgements**

I would like to thank Halle Lowe and Vinay Chandrasekaran for all of their help and support in creating this piece. I would also like to thank Dr. G. Genin for the mechanical background and research techniques he contributed to this work. Additionally, thank you to Dr. M. Zayed, Dr. J. Osbun, and Dr. E. Leuthardt for providing a detailed understanding of the clinical relevance and applications.

**References**

[1] Madigan, J., Murphy, K., Ed., Robertson, F., Ed., 2014, Interventional Neuroradiology. Techniques in Interventional Radiology, "Vascular Access: Guide Catheter Selection, Usage, and Compatibility", Springer, London.

[2] Blanc, Loïc & Delchambre, Alain & Lambert, Pierre. (2017). Flexible Medical Devices: Review of Controllable Stiffness Solutions. Actuators. 6 (23).

[3] Price, H.L., 1966, "Techniques for the Measurement of the Flexural Rigidity of Thin Films and Laminates".

[4] S. Wienecke, C. Braitenberg, H.-J. Götze, 2007, "A new analytical solution estimating the flexural rigidity in the Central Andes," Geophysical Journal International, 169 (3), 789–794.

[5] Kikumoto, M., Kurachi, M., Tosa, V., & Tashiro, H., 2006, "Flexural rigidity of individual microtubules measured by a buckling force with optical traps," Biophysical journal, 90 (5), 1687–1696.

[6] Samanta, Ashis & Basu, Gautam, 2005, "A simple method of measuring flexural rigidity of jute fibre" 85. 33-38.

[7] Sanjay Govindjee, 2012, Engineering Mechanics of Deformable Solids, 01 edition, Oxford University Press.

[8] "Moderately Large Deflection Theory of Beams" Lecture 6, from https://ocw.mit.edu/courses/mechanical-engineering/2-080j-structural-mechanics-fall-2013/course-notes/MIT2_080JF13_Lecture6.pdf

[9] 1966, " I. Mechanical Properties of Catheters." Acta Radiologica. Diagnosis, 5(260_suppl), 11–21.

[10] Stenqvist O, Curelaru I, Linder LE, Gustavsson B., 1983, “Stiffness of central venous catheters,” Acta Anaesthesiol Scand 1983, 27, 153–157.

[11] Bersten, A. D., Williams, D. R. G., & Phillips, G. D, 1988. “Central Venous Catheter Stiffness and its Relation to Vascular Perforation” Anaesthesia and Intensive Care, 16 (3), 342–351.

[12] Eckmann, D.M., 2003, “Variations in epidural catheter manufacture: implications for bending and stiffness” Regional anesthesia and pain medicine, 28 (1), 37-42.

[13] Carey, Jason & Fahim, Atef & Munro, Michael, 2004, “Design of braided composite cardiovascular catheters based on required axial, flexural, and torsional Rigidities.” Journal of biomedical materials research. Part B, Applied biomaterials. 70. 73-81.

[14] C. Chautems, A. Tonazzini, D. Floreano and B. J. Nelson, 2017, "A variable stiffness catheter controlled with an external magnetic field," 2017 IEEE/RSJ International Conference on Intelligent Robots and Systems (IROS), 181-186.

**Appendix A**

**Derivations**

To determine the flexural rigidity, the linear and nonlinear beam theory equations were used in tandem to find values to compare to the actual value. First, the nonlinear beam theory calculations were derived. Equation A1 below shows the general static form for linear and nonlinear beam theory.

$$M = -EI\kappa \tag{A1}$$

Equation A2 below shows an assumption made to determine the static form of Euler-Bernoulli beam theory for linear applications.

$$\kappa = -\frac{d^2w}{dx^2} \tag{A2}$$

To then solve for the flexural rigidity of the beam, the linear form of curvature is substituted into equation and rearranged in Eq. A3 below.

$$EI\frac{dw}{dx} = \int_0^x M(x)dx \tag{A3}$$

Equation A4 shows simplifications made to Eq. A3 based on geometry and the location of the applied force.

$$EI(tan\theta) = \int_0^L Fxdx \tag{A4}$$

Equation A5 shows the final linear form for flexural rigidity after further simplification.

$$EI = \frac{1}{2tan\theta}(FL^2) \tag{A5}$$

To solve the nonlinear application of beam theory for flexural rigidity, the same process is followed with the exception of the curvature, which is replaced with the term shown in Eq. A6.

$$\kappa = \frac{-\frac{d^2w}{dx^2}}{(1+(\frac{dw}{dx})^2)^{\frac{3}{2}}} = \frac{w''}{(1+(w')^2)^{\frac{3}{2}}} \tag{A6}$$

Note that $w'$ and $w''$ represent $\frac{dw}{dx}$ and $\frac{d^2w}{dx^2}$, respectively. By substituting the curvature term ($\kappa$) into Eq. A1, each side can be integrated to solve for flexural rigidity, as shown in Eq. A7.

$$\int_0^L Mdx = \int_0^L EI\kappa dx \tag{A7}$$

By substituting $Fx$ for the moment, the integral can be solved as a function of the length, $L$. Assuming the flexural rigidity ($EI$) is constant along the measured length of the beam, it can be removed from the second integral. Equation A8 shows these results and substitutes the definition of curvature for $\kappa$.

$$\tfrac{1}{2}FL^2 = EI\int_0^L \frac{w''}{(1+(w')^2)^{\frac{3}{2}}}dx \tag{A8}$$

Equations A9 through A12 show the remaining steps to solve the remaining integral. This integral can be solved using u-substitution. The substitution terms for this integral are defined in Eq. 8 below.

$$u = 1 + (w')^2,\ du = 2w'w''dx \tag{A9}$$

Equation A10 shows the remaining integral once the substitution terms are applied. The equation is then simplified.

$$EI\int \frac{w''}{2w'w''(u)^{\frac{3}{2}}}du = EI\int \frac{1}{2w'(u)^{\frac{3}{2}}}du \tag{A10}$$

The remaining $w'$ term can be replaced by $\pm\sqrt{u-1}$, which is derived from Eq. A9. The remaining integral is solved in Eq. A11.

$$EI\int \frac{1}{2\sqrt{u-1}(u)^{\frac{3}{2}}}du \tag{A11}$$

Through u-substitution (setting $v = \sqrt{1-u}$), and trigonometric substitution, the remaining integral can be solved. Equation A12 shows the solution to that integral.

$$EI\frac{\sqrt{u-1}}{\sqrt{u}} = \left[EI\frac{\sqrt{(w')^2+1-1}}{\sqrt{(w')^2+1}}\right]_{x=L} \tag{A12}$$

The remaining solution can be set back equal to the integral of the moment, which was solved in Eq. A8. This is shown in Eq. A13.

$$\tfrac{1}{2}FL^2 = EI\frac{w'(L)}{\sqrt{1+(w'(L))^2}} \tag{A13}$$

By defining $\theta$ as the angle that the free end (at $x = L$) is making relative to horizontal, $tan\theta$ can be substituted into Eq. A12. By rearranging Eq. A12 to solve for flexural rigidity ($EI$), Eq. A14 shows the final nonlinear definition of flexural rigidity for a bending beam.

$$EI = \frac{(1+(tan\theta)^2)^{\frac{1}{2}}}{2tan\theta}(FL^2) \tag{A14}$$

The final forms of both Eq. A5 and Eq. A14 can be nondimensionalized and described by the term $\frac{FL^2}{2EI}$. These results of this nondimensionalization are shown below in Eq. A15 and Eq. A16 for the linear and nonlinear forms, respectively.

$$\frac{FL^2}{2EI} = tan\theta \tag{A15}$$

$$\frac{FL^2}{2EI} = \frac{tan\theta}{(1+(tan\theta)^2)^{\frac{1}{2}}} \tag{A16}$$